Plasmonics (2011) 6:565–580
DOI 10.1007/s11468-011-9237-0

Plasmonic Nanolithography: A Review

Zhihua Xie · Weixing Yu · Taisheng Wang · Hongxin Zhang · Yongqi Fu · Hua Liu · Fengyou Li · Zhenwu Lu · Qiang Sun

Received: 9 January 2011 / Accepted: 23 May 2011 / Published online: 31 May 2011
© Springer Science+Business Media, LLC 2011

Abstract Surface plasmon polaritons (SPPs) has attracted great attention in the last decade and recently it has been successfully applied to nanolithography due to its ability of beyond diffraction limit. This article reviews the recent development in plasmonic nanolithography, which is considered as one of the most remarkable technology for next-generation nanolithography. Nanolithography experiments were highlighted on the basis of SPPs effect. Three types of plasmonic nanolithography methods: contact nanolithography, planar lens imaging nanolithography, and direct writing nanolithography were reviewed in detail, and their advantages and shortages are analyzed and compared, respectively. Finally, the development trend of plasmonic nanolithography is suggested.

Z. Xie · T. Wang · H. Zhang · H. Liu · F. Li · Z. Lu · Q. Sun
Opto-electronic Technology Center,
Changchun Institute of Optics, Fine Mechanics and Physics,
Chinese Academy of Sciences,
Changchun, Jilin 130033, China

Z. Xie · T. Wang
Graduate School of the Chinese Academy of Sciences,
Beijing 100039, China

W. Yu (✉)
State Key Laboratory of Applied Optics,
Changchun Institute of Optics, Fine Mechanics and Physics,
Chinese Academy of Sciences,
Changchun, Jilin 130033, China
e-mail: yuwx@ciomp.ac.cn

Y. Fu (✉)
School of Physical Electronics,
University of Electronic Science and Technology of China,
Chengdu 610054, Sichuan Province, People's Republic of China
e-mail: yqfu@uestc.edu.cn

Keywords Plasmonic nanolithography · Contact nanolithography · Planar lens imaging nanolithography

Introduction

Lithography technique has always been considered as a mainstream of fabrication methods in semiconductor industry for its high throughput and cost effective in comparison to electron beam lithography [1] and focused ion beam writing over the past several decades. Higher throughput, lower cost, higher resolution, and simplification of system configuration are the targets we always pursue. Various types of nanolithography techniques have been explored before, such as electron beam lithography, nanoimprint lithography [2], dip-pen lithography [3, 4], and others. For electron beam lithography, the smallest resolution of less than 10 nm has been demonstrated, but the throughput of this technique is rather low so that it is mainly used for the fabrication of masks rather than mass production. Nanoimprint lithography, with the resolution of less than 10 nm and a high throughput, can be used in mass production. However, as a replication method, there are still some issues for nanoimprint lithography to address. One of the issues is that the residual resist layer after imprinting can arise which may limit its application [5]. Dip-pen lithography has the same disadvantage of low throughput as electron beam lithography. Apart from the aforementioned techniques, photolithography is another important technique for nanolithography. The conventional photolithography techniques for nanolithography include optical projection lithography (193 immersion lithography) [6–8], X-ray lithography [9], extreme ultraviolet lithography [10], zone-plate-array lithography [11–16], and so on. The optical projection lithography is mostly used in industry

due to its high throughput. But with the requirement for smaller feature sizes, conventional optical projection lithography technique cannot meet the resolution requirement anymore because it is diffraction limited. Conventionally, the resolution of optical projection lithography is enhanced by means of reducing the illumination wavelength or increasing the numerical aperture (NA), which brings too much complexities and escalating cost. X-ray lithography can have a high throughput and has demonstrated a 50 nm resolution, but the X-ray lithography system is rather expensive, which urges us to cast about for a lithography system with lower cost to substitute it [17]. Extreme ultraviolet lithography can also obtain a high resolution, but the high cost of light source and complexity of the optical exposure system limit its application in industry for mass production use. As to the zone-plate-array lithography, it is a novel schematic method to be able to expose arbitrary patterns with relative fast speed. However, its resolution is still diffraction limited.

Near-field optical lithography provides a new route to beat the diffraction limit and could achieve a resolution without the limitation in theory. Recently, many sorts of near-field lithography systems have been reported [18–22]. Conventional near-field lithography has achieved sub-50 nm resolution using special masks such as light-coupling mask or phase-shift mask [23]. But one of the main shortcomings of near-field lithography is that the transmittance of the light is extremely low. For the apertures on the mask smaller than illumination wavelength, the amount of the light reaching resist is rather low because most of the light has been diffracted and scattered away. This leads to a considerably long exposure time and low image contrast.

More recently, near-field lithography developed on the basis of surface plasmon polaritons (SPPs) theory has been proposed for the purpose of further improving the resolution of near-field lithography. Surface plasmons (SPs) are collective electrons existing at the interface of the metal and the dielectric [24]. SPs have its unique dispersion relation, which attributes to the resolution beyond the diffraction limit. The dispersion relation is shown by Eq. 1:

$$k_{\mathrm{sp}} = \left(\frac{2\pi}{\lambda_0}\right)\sqrt{\frac{\varepsilon_d \varepsilon_m}{\varepsilon_d + \varepsilon_m}} \tag{1}$$

where, λ_0 is the light wavelength in vacuum, ε_d and ε_m are the permittivities of the dielectric and metal layers, respectively. From the dispersion equation, we can get that the wavelength of the SPs is shorter than the light wavelength in vacuum (λ_0) and the shorter wavelength is responsible for the resolution beyond diffraction limit. Surface plasmons exist in two forms, propagating and localized. On the smooth film, the SPPs wave is propagating as an evanescent electromagnetic wave at the metal–dielectric interface, and is the results of collective oscillations of the conduction free electrons in the metal surface. Generally, SPPs cannot easily be excited for the momentum mismatch between light waves and the waves of the SP. The metal mask with perforations array and proper periods can compensate the momentum mismatch and excite the SPPs. Localized surface plasmon resonance is not propagating at horizontal plane but localized electromagnetic fields near the surface of the isolated nanoparticles [25]. For a single subwavelength aperture, the transmission can be enhanced due to the existence of localized surface plasmon (LSP). As for the periodic aperture array, the transmission enhancement can be explained as the integrated effect of LSP and SPPs [26]. The lithography technique based on surface plasmon theory is called plasmonic photolithography. For plasmonic photolithography, resolution and contrast can be improved significantly due to the extraordinary enhancement of transmittance. Recently, many SPP-based lithography experiments have been conducted. Computational numerical simulations show that the resolution as high as 20 nm can be achieved using the illumination light with 365 nm wavelength [24]. And it seems that plasmonic photolithography has the potential to satisfy the requirements of high resolution, low cost, and high throughput simultaneously. In this article, we will review the typical plasmonic photolithography experiments firstly. Then a comparison of these experiments is concluded. Finally, the development trend of the plasmonic nano-photolithography is put forth.

Plasmonic Nanolithography

Generally, plasmonic nano-photolithography can be categorized into three types in terms of the exposure methods: namely contact nanolithography, planar lens imaging nanolithography, and direct writing nanolithography, respectively. In the following section, we will try to review the plasmonic nanolithography experiments as many as possible by dividing all these experiments into the three types techniques mentioned above.

Plasmonic Contact Lithography

Plasmonic contact lithography is a modified form of evanescent near-field optical lithography designed to improve subwavelength image quality [27]. In this method, the photoresist is exposed by SPPs which is originated from the metal mask. As the SPPs can only propagate tens of nanometers beneath the metal film, the intimate contact between the mask and photoresist film is necessary. Many efforts have been devoted to the exploitation of this technique.

In 2005, Srituravanich et al. experimentally demonstrated nanolithography with a half-pitch resolution down to 60 nm using a 2D holes array perforated through Ag mask [24]. A filtered mercury lamp with a radiation peak at 365 nm was employed as the illumination source. The schematic diagram is illustrated in Fig. 1a. The mask is composed of an Ag layer perforated with a 2D periodic holes array patterned and sandwiched between quartz and OmniCoat layers (refractive index is 1.48 and 1.57, respectively). The Ag film has a thickness of 40 nm, and the holes array has a periodicity of 120 nm and each hole has a diameter of 60 nm. It is noted that an adhesion layer of 3 nm thick titanium film was added between the Ag and quartz substrate so as to increase adhesion of the Ag film and reduce the surface roughness. With this configuration, small feature sizes are fabricated in Ag film with significantly low surface roughness as illustrated in Fig. 1b. A 15 nm thick spacer layer of OmniCoat is spin coated on the patterned Ag film. A negative photoresist (SU-8) is directly spin coated on top of the spacer layer and polymerized on the mask to eliminate the gap variation between the mask and photoresist in the photolithography process. 2D holes array with the feature size as small as 60 nm (equivalent to $\lambda_0/6$) has been obtained with the exposure does of 80 mJ/cm^2 and illustrated in Fig. 2. Feature size obtained on photoresist is the same size with the patterns on the mask. Therefore, the resolution is mainly limited by the resolution on the mask. The pattern fidelity is significantly high due to the particularly short propagation length of SPPs in this case (<20 nm). It is noted that Al film can also be employed as the mask since it can excite the SPPs in the ultraviolet (UV) range and a sub-100 nm dot array pattern with a 170-nm period has been successfully obtained using a 365-nm wavelength light source by Srituravanich et al. [28]. But simulation results calculated by use of commercial finite-difference time-domain software (Microsoft Studio) showed that under the plane wave illumination (λ=365 nm), the electric field transmitted through the Ag holes array has a significant enhancement on the field strength and tight confinement of the field distribution compared with that of the Al holes array [29]. Therefore, it can be concluded that for the 365 nm wavelength irradiation, Ag film can realize a better pattern than that of Al film.

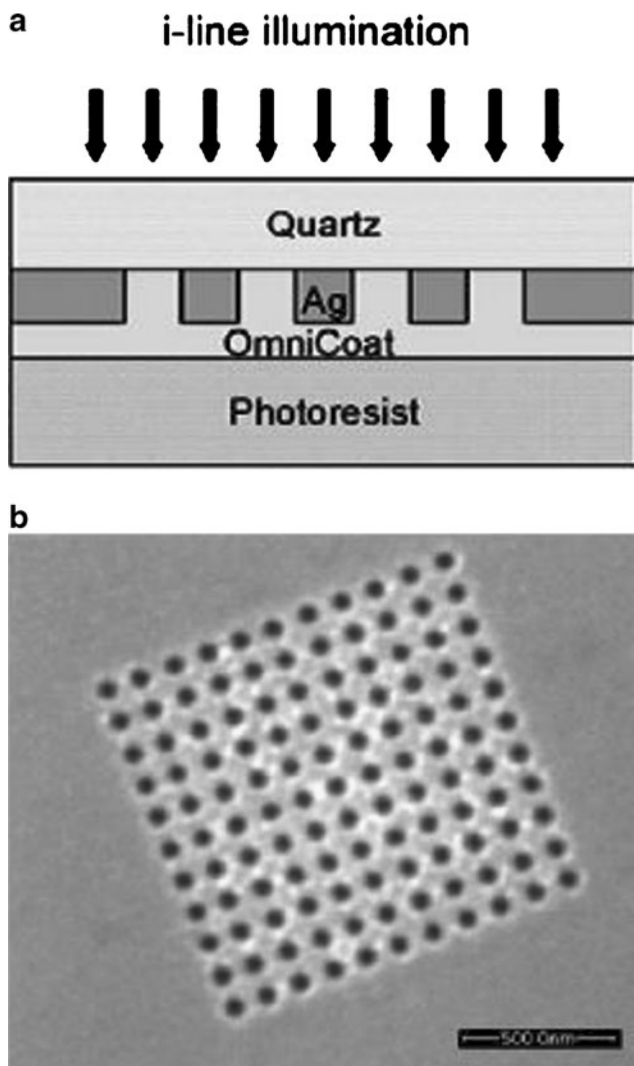

Fig. 1 **a** Schematic of lithography setup designed by Srituravanich et al. **b** The silver mask with hole array used in this experiment. Reprinted with permission from [24]

Shao et al. exploited a surface plasmon-assisted nanolithography system similar to the one discussed above [30], whereas a UV lamp is employed to provide light irradiation. The photomask is made from a 70-nm thick titanium film with the patterns of grating structures and ring apertures. The mask is intimately in contact with the photoresist without the spacing layer. An 80-nm thick titanium shield is added in between the photoresist and the substrate to focus the light intensity in the photoresist so as to achieve nanoscale patterning with high density and absorb the light as it reaches the substrate. In this experiment, both the number of apertures and the periodicity are the critical factors affecting the lithography results. The grating with a period of 400 nm was transferred fairly well and the pattern obtained in the resist has a height of ~35 nm. However, the pattern that has a single aperture was not transferred to the resist, which indicates that the performance of the mask mainly depends on design of the aperture shape and aperture size in the mask.

Zayats and Smolyaninov proposed a new method to achieve strongly enhanced transmittance of an individual subwavelength aperture [31]. They demonstrated that the optical transmission of an individual subwavelength aperture in a multi-layered metal film was shown to be strongly enhanced compared with that of a homogeneous single-layered metal film due to the light coupling to surface

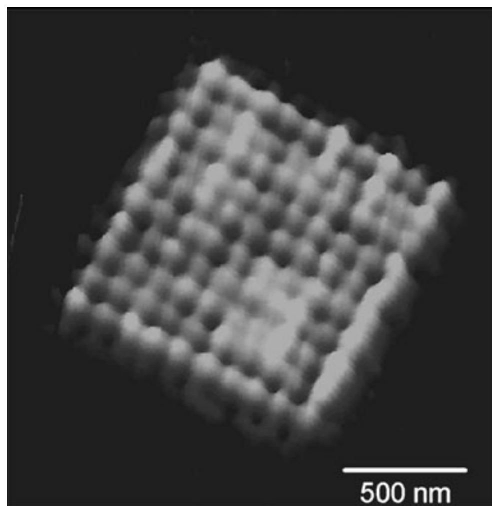

Fig. 2 AFM image of the exposure pattern. Reprinted with permission from [24]

plasmon excited by a periodically structured film. This method enhances optical transmission in up to two orders of magnitude in comparison to an aperture with the same size perforated in a homogeneous film. Moreover, the multi-layered metallic film can be conventionally prepared with well-developed thin-film deposition techniques. Such structures are robust and are easy to fabricate due to the absence of the fabrication of complex periodic structure required by conventional single-metal-film plasmonic mask. This proposal can be used in lithography and it may deliver a better lithography result. The application in lithography is going to be demonstrated experimentally. Similarly, a photolithography scheme using a designed metal-dielectric multilayer was proposed to generate sub-wavelength feature size [32]. Generally speaking, the patterns fabricated in photoresist are identical to the patterns in mask for the scheme. However, numerical experiments show that a much smaller feature size could be obtained such as for a 400-nm period grating structure in a mask, a 67-nm period grating structure can be fabricated in photoresist.

The utilization of an array of holes in noble metals shows transmission enhancement with the aid of the resonant excitation of surface plasmon, while the spatial resolution is somehow sacrificed by the period of the holes array [33]. Recent research showed that sharp-ridged apertures in metal, such as bowtie apertures or antennas, C-, H-shaped apertures and others, may realize a better result. The bowtie antenna was an important aperture type and was proposed firstly by Grober et al. and used as a near-field optical probe with high transmission efficiency at microwave frequency [34]. Subsequently, a lot of efforts have been devoted to the research of the bowtie structure. And the applied frequency was extended to visible and even UV range. Highly confined hot spots with enhanced intensity were observed in the near-field of bowtie structures due to the localized surface plasmon resonance. It has been applied in many domains due to the enhanced transmittance of bowtie structures, such as high efficiency excitation of plasmonic waveguides [35], high-harmonic generation, and so on [36]. Recently, it has been successfully applied in nanolithography as a novel method to improve the resolution.

A bowtie aperture is the counterpart of a bowtie antenna as shown in Fig. 3. Both of two structures consist of two arms and a small gap formed by two sharp tips pointing toward each other. The simulation results indicate that the resonance at 505 nm, the corresponding field intensity at the bowtie apex is more than 15,000 times of that of illumination field, which is comparable to the bowtie antenna [37]. But the actual performance would be greatly affected by the aperture size, metal material, wavelength, polarization, and some other factors. A mask with bowtie apertures can be used in contact lithography and a fine result has been demonstrated. Xu et al. firstly applied the bowtie aperture in plasmonic contact lithography experimentally and 2D holes with feature size of sub-50 nm were resolved using the bowtie apertures [38]. The bowtie apertures with a 30-nm gap size fabricated in 150-nm thick Al film coated on quartz substrates were employed as the mask. Al was selected as the mask material because of its small skin depth and high reflectivity. The mask was illuminated by a diode-pumped solid-state 355 nm laser beam polarized in the direction across the gap. The experimental setup is illustrated in Fig. 4. The experiment was performed in a class-10 clean room rating glove box to minimize the contamination and to prevent the environmental light from exposing the photoresist. With a 3×UV objective lens, the laser beam is focused into a 110 μm diameter spot on the mask. The polarization of the laser beam is directed across the gap of the bowtie aperture. A positive photoresist (Shipley S1805) was used in this experiment. As the depth and dimension of holes were directly affected by the exposure time, therefore, precise control of exposure time is required. The exposure time is controlled using an electric shutter with millisecond timing

Fig. 3 Schematic of bowtie aperture (*left*) and antenna (*right*). Reprinted with permission from [38]

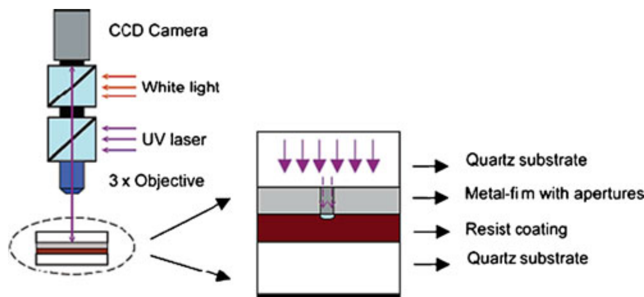

Fig. 4 Schematic diagram of the experimental lithography system designed by Xu et al. Reprinted with permission from [38]

precision. As a result, subdiffraction-limit lithography holes as small as 40×50 nm were obtained in the positive photoresist with a 1.3-s exposure time.

Recently, Ueno et al. explored a new plasmonic lithography method using the localized field of nanogaps [39]. The mask consisting of pairs of rectangular gold nanoblocks which are separated by nanogaps fabricated on glass substrate. In this experiment, a femtosecond laser (Tsunami, Spectra Physics) with a central wavelength of λ_L=800 nm, a pulse length of τ_P=100 fs, and a repetition rate of f=82 MHz were employed as the illumination source. The beam is normally incident with respect to the substrate (*x*–*y* plane) and is linearly polarized along the diagonal of the blocks.

The schematic diagram of gold nanoblock pairs was illustrated in Fig. 5. The nanoblocks are rectangular gold cuboids with a size of 80×80×35 nm arranged into pairs oriented along a common diagonal parallel to the *x*-axis with the gap size of 4 nm. The mask consists of large periodic arrays of nanoblock pairs arranged on a square lattice with a period of 400 nm.

An experimental setup with 70-nm thick positive TSMR V-90 photoresist film is illustrated in Fig. 6a. The resist was spin coated on a glass substrate. The substrate is brought into direct contact with the top surface of the nanoblocks. The exposure is expected to occur in regions of photoresist adjacent to the nanogaps. And the experimental result is illustrated in Fig. 6b. For a lower irradiance of 0.6 W/cm^2, only the regions adjacent to the nanogaps are exposed and it was reported that single pit with a typical lateral size of about 5 nm has been obtained (the inset image of Fig. 6b), which is about 0.6% of the laser wavelength. The main image of Fig. 6b is the pattern obtained with an exposure of 60 W/cm^2. This method can be conducted with other geometries of metallic nanostructures. The research group has also demonstrated a mask with structures consisting of pairs of gold strips with a dimension of 1,000×100×36 nm separated by 20-nm wide nanogaps and arranged with a period of 600 nm on the substrate. Series of lines with an average width of 40–50 nm extending along the entire length of the stripes was recorded. In this configuration, laser beam is incident on the photoresist from the backside of the substrate that was coated by the same resist. In comparison to the nanoblocks mask, this schematic has a lower enhancement factor and a higher contrast.

From above, we can conclude that the bowtie structure-based lithography and the nanogap-assisted lithography technique have a better resolution compared to the mask with holes array. Therefore, these two types of techniques may have a brighter future.

In addition, it is worth to mention that some researchers have tried to use spherical or nonspherical particles as masks for nanopatterning as well [24, 40]. In this case, the hole size and lattice period could be tuned independently.

Although the transmittance of plasmonic nanostructure has been greatly enhanced, plasmon damping originated from intrinsic metal absorption limits the achievable aspect ratio of the fabricated structures. To obtain higher field depth, K. Sathiyamoorthy proposed a novel concept of employing the dye medium to enhance plasmon propagation by compensating intrinsic loss associated with metal [41]. In this proposal, polymethylmethacrylate (PMMA) doped with the dye material was employed as the mask substrate. Simulation results show that a 14.5-fold of field enhancement in the PMMA/dye medium can be obtained compared to that of the bare PMMA. In addition, Kid et al. exploited metal nanoparticle arrays for near-field optical lithography and spot sizes ranging from 30 to 80 nm with exposure depth ranging from 12 to 45 nm have been achieved using broad beam illumination with visible light and standard resist [42].

Plasmonic contact lithography has the advantages of high resolution and high throughput. But the mask used in this technique is rather expensive and the fabrication process is very complex. In addition, the intimate contact between the mask and substrate will result in the contamination of the mask and thus reduce lifetime of the mask. These intrinsic shortcomings will constrain its applications in mass production of industry.

Planar Lens Imaging Nanolithography

Planar lens imaging nanolithography is the method to use the so-called "superlens" positioned underneath the mask to project the nanopatterns through the mask onto the image

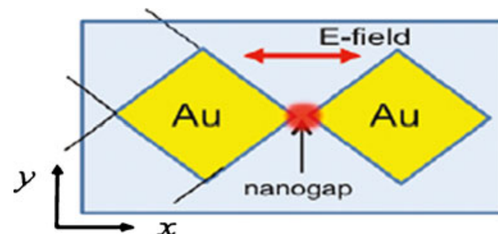

Fig. 5 Schematic of gold nanoblock pairs. Reprinted with permission from [39]

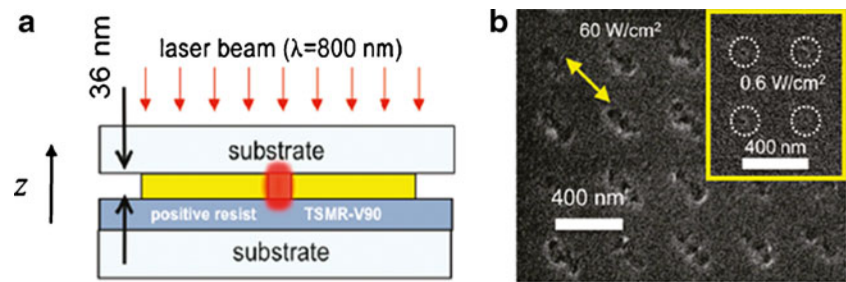

Fig. 6 **a** The setup designed by Ueno et al. **b** SEM images of periodical pits in the photoresist. Reprinted with permission from [39]

plane (normally in photoresist) which is about tens of nanometers under the superlens to make patterns in photoresist. The concept of "superlens" was theoretically proposed by Pendry first [43]. He predicted that a slab of negative refractive index material (NIM) has the power to project the near-field image with subdiffraction limit onto the image plane because the negative index medium can bend light into a negative angle with respect to the surface normal. The property of NIM can make a slab of NIM a "superlens". The principle of superlens is illustrated in Fig. 7. Light formerly diverging from a point source is set in reverse and converges back to a point when transmitting through the superlens as illustrated in Fig. 7a. The near-field evanescent waves can be strongly enhanced across the lens as illustrated in Fig. 7b [44]. This enhancement is assisted by the excitation of surface plasmons on the metal film. The materials with negative refractive index do not exist in nature. Although many approaches have emerged to obtain artificial NIMs, such as photonic crystals [45, 46] and metamaterial nanostructures [47–52], there are still challenges for the NIM to be applied for photolithography so far. Professor Pendry proposed that the ultrathin Ag film whose permittivity has a negative real part and small positive imaginary part can be employed as the superlens. The physical mechanism of this type of superlens is that the imaginary part of the metal film was ignored because the absolute value of real part is far larger than that of the imaginary part [53]. The small imaginary part means that the amount of the absorbed light is too less to be considered in practice. The superlens is capable of focusing all Fourier components from the objects onto a 2D image with a resolution far beyond the diffraction limit [54]. Most superlenses were put forth based on the condition that the superlens and the surrounded dielectric have a matched permittivity ($\mathrm{Re}(\varepsilon_m)=-\varepsilon_d$) at the working wavelength, where the ε_m and ε_d denotes the permittivity of metal and dielectric, respectively [55]. For different superlens materials, different wavelengths are chosen so that the superlens is index matched to dielectric medium. Therefore, the superlenses based on bulk metal can only operate at a single frequency for the given surrounded dielectric. However, Cai et al. proposed a new superlens which composes of metal and dielectric and the superlens can operate at practically any desired wavelength in the visible and near-infrared ranges by tuning the metal-filling factor [56]. This proposal has been verified by the simulations but not been demonstrated in experiment yet. Ag is an ideal metal material in UV range which can be used as the superlens for its low absorption. Experiments have shown that evanescent waves can be enhanced significantly in Ag slabs [57]. It is predicted that the image with a resolution of about $\lambda/20$ can be realized in principle with the proper superlenses [58]. But the metal absorption in the lenses and the dispersive nature of the lenses limited the spatial resolution. The spatial dispersion will remain and limit the resolution even if the absorption is reduced or compensated by the

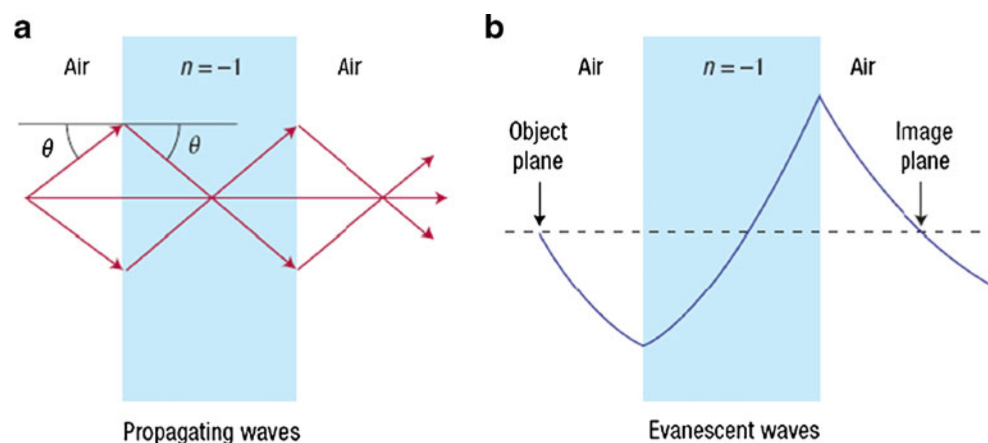

Fig. 7 **a** An NIM flat lens brings all the diverging rays from an object into a focused image. **b** The NIM can enhance the evanescent waves across the lens. Reprinted with permission from [44]

optical gain [55]. Therefore, it is difficult to achieve the theoretical resolution in practice.

Many experiments have been implemented to confirm this prediction. Melville demonstrated optical imaging through a thin planar Ag layer with a thickness of 120 nm using a light source with a wavelength of 341 nm in 2004 [59]. Feature size as small as 350 nm (with 700 nm period) was well resolved. Subwavelength imaging was not demonstrated because the Ag lens is not thin enough. In 2005, a modified system with a thinner lens with a thickness of 50 nm was demonstrated to be able to resolve a subwavelength image [60]. Where, the superlens structure consists of 25 nm PMMA/50 nm Ag/10 nm SiO_2. A 350 W mercury lamp with a 365 nm wavelength, which gives an intensity of 6.7 mW/cm^2 was employed as the light source. The substrate is a 1-in. diameter silicon wafer. The image of a grating with a period of down to 145 nm has been successfully resolved. Numerical simulation shows that the smallest resolution that can be achieved using this method is 40 nm. A comparison between 50 nm single- and double-layer lens with two 30-nm layers was made by Melville in 2005 [61]. Gratings with 170 nm period have been resolved for the double-layer lens. The results demonstrated that double-layer lens has a shorter exposure time. The enhancement of the transmission has been achieved through the double-layer stack despite the increase in total thickness. The resolution limit for the double layer is no less than a single layer with the same total Ag thickness. However, double-layer lens does not always lead to better imaging performance because of two reasons. One is that the lens has a specific resonance and the feature of the image will be distorted at spatial frequencies out of resonance. The other is that the double-layer lens has an increasing attenuation of the DC component of transmitted images, which reduces the image fidelity, particularly for dark-line features [62].

In 2005, Zhang et al. demonstrated subdiffraction-limited imaging with a 60 nm half-pitch resolution [63]. The setup of their experiment is shown in Fig. 8. As can be seen in Fig. 8, a set of embedded objects are inscribed into the 50-nm thick chrome (Cr) film. Left side is an array of 60-nm wide slots with a 120-nm pitch, and right side is an arbitrary object “NANO”. The line width of the “NANO” object (illustrated in Fig. 9a) is 40 nm. The Ag film is separated from the objects by a 40-nm thick PMMA layer. Following the PMMA layer is photoresist. A UV light with a wavelength of 365 nm is employed as the light source. A control experiment in which the Ag film is replaced by PMMA was conducted as well for comparison. A 120-nm thick negative photoresist [NFR 105 G, Japan Synthetic Rubber Microelectronics (JSR Micro)] is coated on Ag film to record the near-field image. The substrate is then exposed under an I-line filtered mercury lamp with flux of

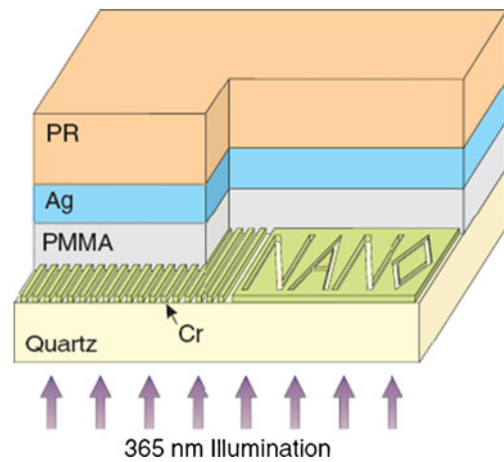

Fig. 8 Optical superlens designed by Zhang’s group. Reprinted with permission from [63]

8 mW/cm^2 and an optimal exposure time of 60 s. Using this method, the arbitrary pattern of “NANO” (illustrated in Fig. 9b) and 1D lines with width of 60 nm (about $\lambda/6$; illustrated in Fig. 10a), with typical average height of 5–10 nm, was fabricated in photoresist. The control experimental results are shown in Figs. 9c and 10b. To make a comparison, the cross-sectional line width of letter “A” patterned in both experiments was measured. In the experiment with the superlens, the line width was about 89 nm while in the control experiment; the full width at half-maximum line width is 321±10 nm. Apparently, the line width obtained with the superlens beats diffraction limit but is still larger than the width of the objects in the masks. The experimental results clearly demonstrated the imaging improvement using the superlens. The same setup was utilized to realize the imaging of a 50 nm half-pitch object at $\lambda_0/7$ resolution [64].

Currently, the best resolution achieved by the planar lens lithography is about 30 nm. And such a resolution has been demonstrated by Du et al. and Chaturvedi, respectively, using different methods. They employed the localized surface plasmon mask composed with polydimethylsiloxane (PDMS) soft mold and thin Ag film serving as the “superlens” to realize a 30-nm resolution [23]. The PDMS was selected as the mask material due to its two unique advantages: the transparent property for transporting light with a high transmittance and the soft property which assures the intimate contact between the mold and the metal film. TM polarized UV light with wavelength of 365 nm was used to expose the resist. An Ag layer with a thickness of 18 nm served as the superlens and resist (AR-3170) with a thickness of 100 nm was used. After 15-s exposure and 20-s development, the fine groove patterns with a dimension of 30 nm (about 1/12 of the exposing wavelength) and a depth about 20 nm were

Fig. 9 **a** FIB image of "NANO" object. **b** The developed image with silver superlens. **c** The image in the control experiment. Reprinted with permission from [63]

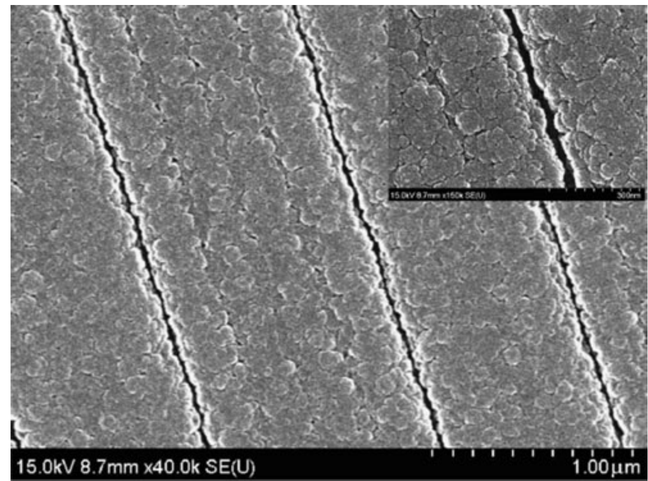

Fig. 11 SEM photography for a lithographic result fabricated by using the LSP lithographic method with the PDMS soft mold in 2 and 0.8 μm line width. The *inset* is a magnified image highlighting the achieved minimum feature size of 30 nm. Reprinted with permission from [23]

obtained in photoresist. The patterns with a 30-nm width are illustrated in Fig. 11.

Another method using smooth and low loss Ag optical superlens capable of resolving features at 1/12 of the illumination wavelength with high fidelity has been demonstrated by Chaturvedi et al. [65]. The setup used by them is illustrated in Fig. 12a, where an array of chrome gratings with 40 nm thick and 30 nm half-pitch serve as the object. The Cr grating was patterned using nanoimprint lithograph method. Then, a 6-nm thick spacer layer was deposited on top of the object as the planarization layer to reduce the surface modulation below 1.3 nm. To enhance the contrast, a 35 nm thick Cr window layer is patterned on top of the spacer layer using photolithography. Then 1 nm thick Ge and 15 nm thick Ag are evaporated over the

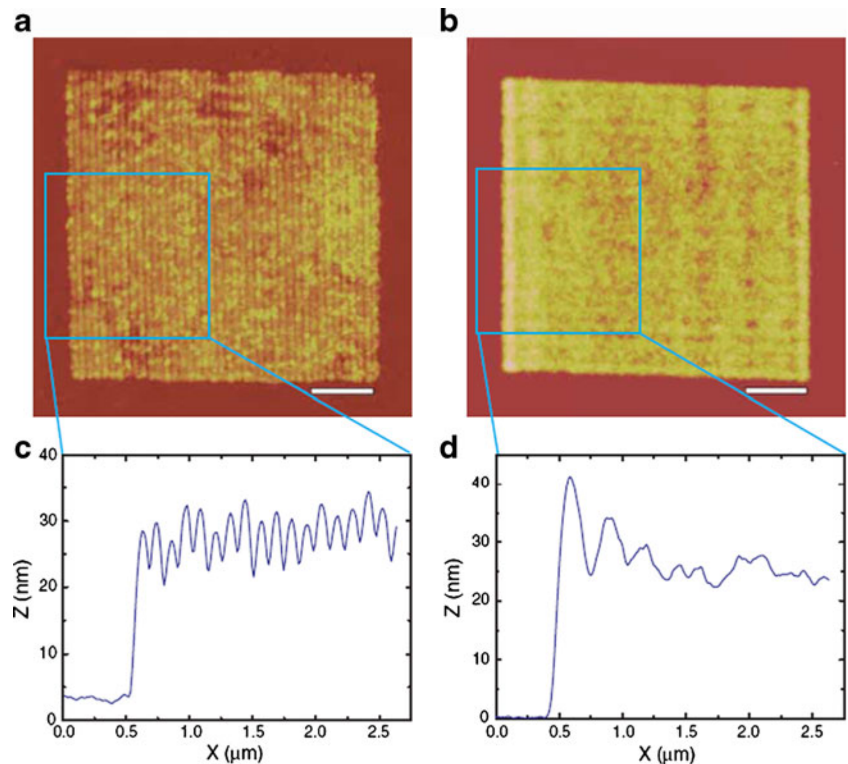

Fig. 10 **a** 1-D image patterned with the superlens. **b** 1-D image patterned without the superlens. **c** The averaged cross-sectional profile of Fig. 10a. **d** The averaged cross-sectional profile of Fig. 10b. Reprinted with permission from [63]

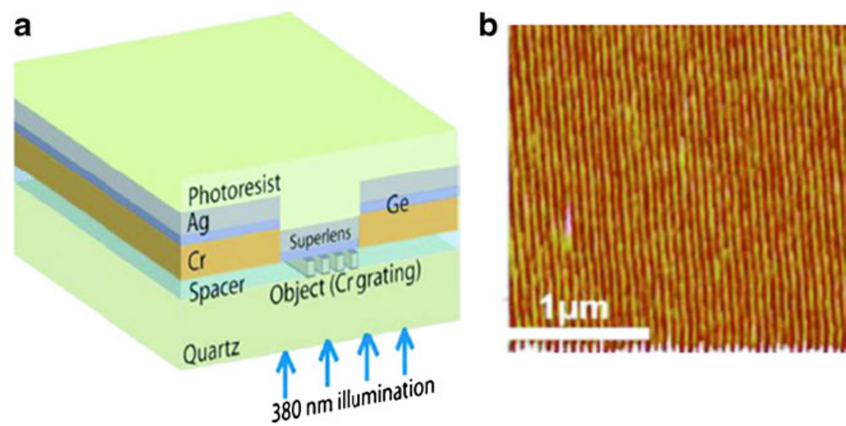

Fig. 12 **a** Schematic drawing of a smooth silver superlens with embedded 30 nm chrome grating designed by Chaturvedi et al. **b** The image of the 30 nm half-pitch Cr grating area recorded on the photoresist layer after exposure and development. Reprinted with permission from [65]

window layer followed by coating with a thick layer of photoresist (NOA-73). The Ge layer is introduced to improve the Ag film surface morphology and make the surface roughness less than 0.8 nm. UV-LED light with a wavelength of 380 nm and a power of 80 mW was employed as the light source. In their experiments, 30 nm half-pitch patterns were obtained in photoresist with an exposure time of 120 s. The experiment result is illustrated in Fig. 12b.

Lately, Zhong Shi proposed a method using a 193 nm Al film-based superlens with index-matching layer. Their simulation indicated that 20-nm resolution can be resolved by the introduction of an "index matching layer" between metal layer and the dielectric layer [66, 67]. The proposed 193-nm superlens may provide an alternative way to reach the 22-nm lithography node. In addition, Xu et al. proposed a metal-cladding superlens to effectively localize the surface plasmons for projecting deep subwavelength patterns [68]. In this configuration, an additional Ag layer was inserted between the photoresist and the substrate. With this special configuration, both the intensity contrast of the interference pattern and the image can be remarkably improved.

For planar lens nanolithogrpahy, the light source is an important factor affecting the experimental results. A comparison about the illumination light with broadband and narrowband has been made experimentally by Blaikie. The results show that broadband light source offers the advantage of shorter exposure time and higher throughput while the depth of the pattern in the resist and the degree of line edge roughness are almost the same as that obtained by narrowband source. However, the resolution of the former is not good as that of the latter due to the dispersive nature of the broadband light source which will result in the aberrations of the planar lens [61]. Therefore, the choice of light source is crucial for planar lens lithography experiment.

The near-field planar lens lithography relaxes the rigid request for intimate contact between mask and substrate to a certain extent. Therefore, damage to the mask due to the intimate contact can be reduced. But the superiority of the technique is still restricted because the image plane is located in the proximity of the superlens (normally the working distance is a few tens of nanometers or even less). Hence, the far-field superlens which can form subdiffraction limit image in far field of the superlens was proposed and experimentally demonstrated by Liu et al. [69]. The far-field superlens consists of a conventional superlens and a nanoscale coupler. The coupler can convert evanescent wave into propagating wave by shifting the incident field wave vector into various diffraction orders and selectively enhance the evanescent waves from the object [70]. In their experiment, an optical microscope (Zeiss Axiovert mat 200, 100× oil immersion objective, NA=1.4) was used to illuminate the object with a 377-nm wavelength light source, combining with the far-field superlens, 50-nm width lines separated by 70 nm has been recorded by CCD. The experiment has successfully demonstrated the imaging ability of the far-field superlens, showing the potential to be applied to nanolithography.

Planar lens lithography has the advantage over the contact lithography at some aspects. However, it is still mask-based nanolithographpy technology. Therefore, it has all the disadvantages brought by the masks. In the next section, we will introduce the maskless nanolithography method based on plasmonics, i.e., plasmonic direct writing nanolithography method.

Plasmonic Direct Writing Nanolithography

The techniques mentioned above are all mask-based lithography. As well-known, the fabrication of the mask with nano-feature size is complicated, time consuming, as well as with very high cost. It was reported that the cost with a set of mask for developing a new product for 193-nm immersion lithography is normally more than 1 million dollars [71]. Moreover, mask-based lithography is not flexible because it is only able to fabricate the specific

patterns defined by mask. Considering the aforementioned disadvantages, more and more attention is paid to direct-writing lithography which is more flexible and can be used to fabricate arbitrary patterns. Scanning probe lithography [72–77] is an important lithography technique belonging to direct writing lithography. The critical component of scanning probe lithography is the scanning probe [78], which is used to transmit light toward the tip of a tapered plasmonic waveguide to expose the resist [79]. Various types of probes have been investigated. Solid immersion lens can also be used as the scanning probe [71, 80, 81]. The scanning microscope probe is the most commonly used near-field scanning probe [82, 83]. Conventional scanning probe lithography utilizes optical fiber with tapered tip as probe. The scanning microscope probe, which is coated with a metal to prevent leakage of the electric field laterally through cone section of the probe, was employed as the scanning probe to expose the photoresist beneath the probe tip [84–86]. Some experiments demonstrated that metal thin film under the probe can also be etched utilizing the photo-thermal effect [87–89]. The photo-thermal effect occurs owing to absorption of the light with high-energy density [90]. Conventional scanning probe lithography, both using solid immersion lens and scanning microscope probe, has their intrinsic disadvantages. For the solid immersion lens, the resolution would be limited by the diffraction limit and for the scanning microscope lithography, the transmittance efficiency of the aperture is so low that the throughput of patterning is too low to be applied for industrial applications [91]. Plasmonic direct writing lithography, which is a promising technique due to its subdiffraction resolution limit, can be defined as an extension of the scanning probe lithography. In this technique, resist is scanned and exposed by the superfocusing light spot focused by the plasmonic lenses. Many plasmonic direct writing systems are an integration of conventional probe (solid immersion lens or scanning microscope probe) and plasmonic subwavelength device. Zhang's group demonstrated a practical plasmonic near-field scanning optical microscopy system (NSOM) experimentally for near-field lithography for the first time [92]. The conic plasmonic lens demonstrated by them consists of a subwavelength aperture at the apex of the cone surrounded by concentric through rings in an Al thin film deposited on a tapered fiber tip, as shown in Fig. 13. The cone angle was set to be 75° and simulation results show that the optimal sizes for aperture diameter, ring periodicity, ring width and Al layer thickness are 100, 300, 50, and 80 nm, respectively. The working wavelength was selected as 365 nm. During the lithography, the laser beam was coupled into the near-field scanning microscope tip to expose the positive photoresist (IX965G, JSR Microelectronic Inc.) on a Si substrate. By using this method, tight focus of approximately a 100-nm beam spot was obtained at the center of the circular grating. Simulation results show that light intensity at the focal point was enhanced ×36 with respect to the intensity through a single aperture due to constructive interference of SPPs. The NSOM probe can also be integrated with ridged apertures such as C-shape, H-shape, bowtie-shaped apertures, and so on. This type of integration requires a flat surface on top of the NSOM probe. The NSOM probe with a bowtie aperture has been demonstrated recently [93, 94]. Experiments have shown that bowtie apertures can both increase the transmission efficiency and shrink the focused light spot size. Murphy-Dubay et al. reported their experimental demonstration of field enhancement of bowtie-shaped apertures integrated with NSOM probe and consistent lines with width of as small as 24 nm were written on resist using the NSOM probes integrated with the bowtie apertures [95]. In this experiment, 800 nm Ti: sapphire femtosecond laser was employed as the light source and thin Al film with a thickness of 120 nm was selected as the bowtie aperture material due to its small skin depth and high reflectivity. But in the experimental process, the probe is required to be in intimate contact with the substrate, which is detrimental to the probe because it will cause abrasion. Although utilization of the probe integrated with a metal film can provide a satisfying result, it has inherent shortage of thermal effect due to the thermal expansion caused by the partial energy absorption by the metallic film, which prevents it from some specific applications [96, 97].

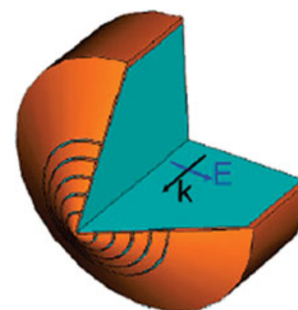

Fig. 13 Schematic drawing of the conic plasmonic lens. Reprinted with permission from [92]

Kim et al. proposed a plasmonic lithography technique with bowtie aperture contact probes [98]. The bottom surface of the probe is covered with a 10-nm thick silica glass film for the gap control. In this method, a relative high-speed patterning without external gap distance control can be realized. The experimental setup is illustrated in Fig. 14. The bowtie aperture with the smallest gap of 20 nm was employed to excite plasmon wave. In this experiment, a conical shape solid immersion lens with a flat surface with 30 μm diameter on top was employed. A 120-nm Al film was coated on the flat surface and a thin Cr layer of 2 nm thickness is added to ensure the adhesion between the Al film and the glass substrate. Bowtie nano-apertures with about 140-nm outline dimension were formed on the metal film by use of focused ion beam (FIB) lithography. A 300-

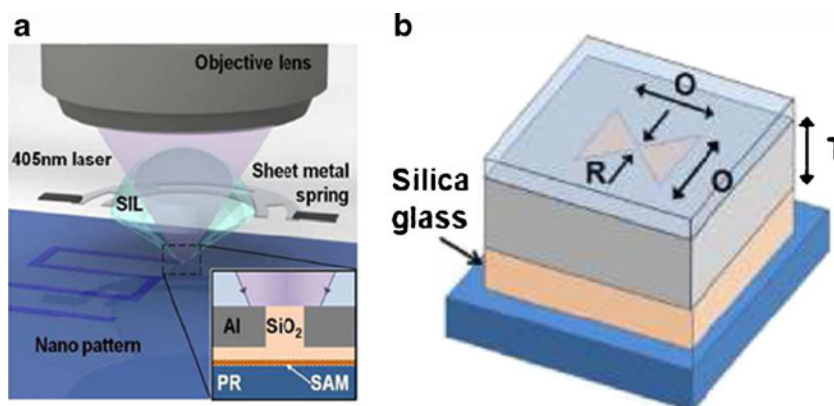

Fig. 14 **a** The structure of the direct writing probe designed by Kim et al. **b** A bowtie aperture designed with silica glass as the map material. Reprinted with permission from [98]

nm thick silica glass film was deposited on the Al film with a subsequent process of FIB milling to reduce the silica glass film thickness down to 10 nm. The use of the silica glass is not only for the control of the gap between the probe and photoresist but also for the protection of aperture from contamination. A single atom self-assembled film was coated on the surface of SiO_2 film to reduce the friction between the probe and the photoresist during scanning. In this experiment, the probe is in intimate contact with resist by means of applying a certain pressure (13±2.5 μN) while the substrate was fixed on nanometer-precision stage. A positive photoresist (Shipley S1805) with 400-nm thickness was coated on the substrate. In this experiment, the solid immersion lens is coupled with a high NA (0.8) objective lens (Nikon CFI LU Plan Epi ELWD ×100) to focus a diode laser beam of 405 nm wavelength onto the nano-aperture. The spot size focused by the solid immersion lens is estimated to be 340 nm. Then the nano-aperture excites surface plasmons to expose the photoresist. The laser source (CrystaLaser, BCL-025-405S) has a polarization-maintaining optical fiber to keep the degree of the polarization at about 0.98. The nano-patterns can be fabricated in resist by scanning the stage beneath the optical probe. The smallest line width of 50 nm illustrated in Fig. 15a can be realized when the polarized laser light with 405 nm wavelength and a power of 0.5 mW was employed using this method. When the laser power is set as 1.25 mW, the lines with a width of 150 nm and a pitch of 1 μm can be fabricated, as shown in Fig. 15b. The system has a highest throughput of 10 mm/s.

Srituravanich et al. in the University of California, Berkeley reported another promising new method with a high throughput [99]. The technique is to use a flying plasmonic lens to focus the surface plasmon wave on a substrate rotating with high speed. The principle of their experiment is illustrated in Fig. 16. In this experiment, a UV continuous-wave laser was focused down to a spot of several micrometers onto a plasmonic lens, which is then further focused into a sub-100 nm beam spot to expose the spinning disk for writing arbitrary patterns. An inorganic TeO_x-based thermal photoresist deposited on a glass disk was employed. A setup called “plasmonic flying head”, on the back surface of which is the fabricated plasmonic lens, was employed as the direct writing probe. The plasmonic lens consists of a concentric ring grating with a through hole in the center. The plasmonic lens was illustrated in Fig. 17. As the subwavelength spots are only produced at the near field of the plasmonic lens, the distance between the plasmonic lens and resist has to be controlled at about 20 nm. To meet this request, a method of a self-spacing air bearing that can fly the plasmonic lens at just 20 nm above the substrate was adopted. The substrate is spinning at

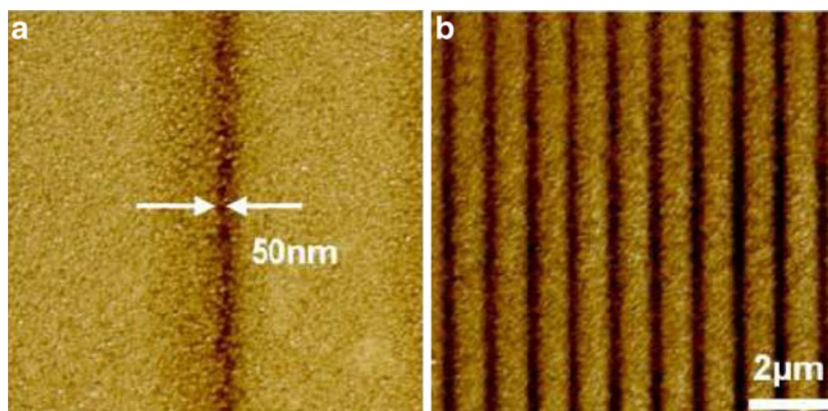

Fig. 15 **a** A *single line* of 50 nm width recorded at speed of 10 mm/s. **b** *Multiple line* pattern of 150 nm width with 1μm pitch. Reprinted with permission from [98]

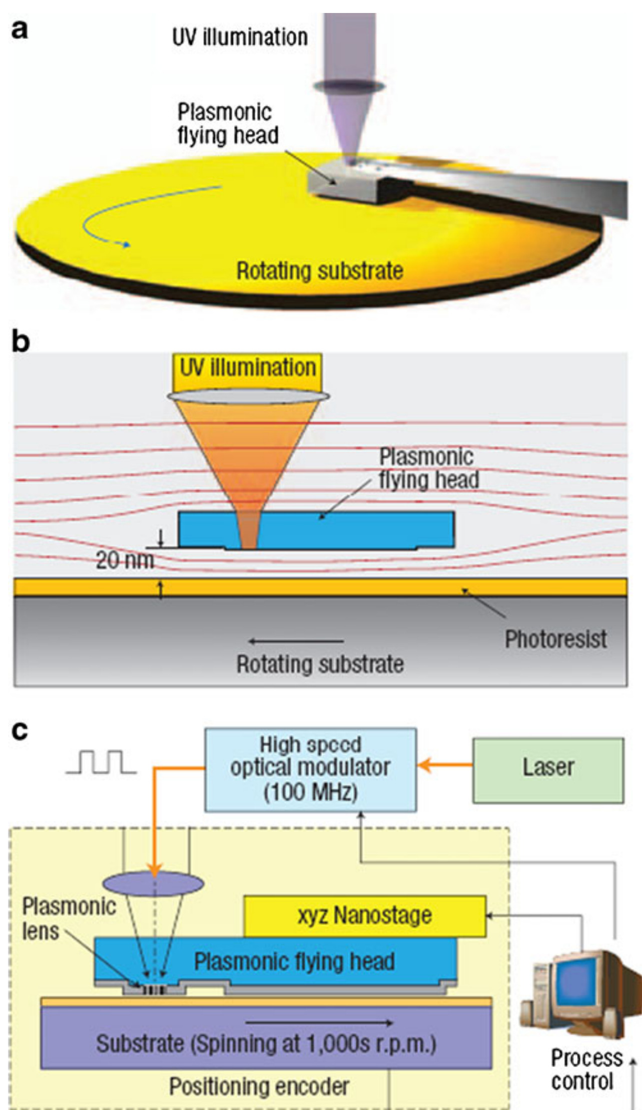

Fig. 16 **a** The schematic showing the plasmonic lens focusing the light onto the rotating substrate. **b** The plasmonic head flying 20 nm above the rotating substrate. **c** Schematic of process control system. Reprinted with permission from [99]

speeds of between 4 and 12 ms^{-1}. The experiment demonstrated that the distance can be controlled within 20±2 nm by using this method. Apart from the rigid distance control, the parallelism of the plasmonic lens and the substrate is also needed to be controlled precisely to ensure the exposure uniformity. A line width of 80 nm with the writing speed of 10 m/s has been demonstrated. According to the authors, if 1,000 plasmonic lens were adopted at the same time, a 12-in. wafer can be processed in just 2 min. Therefore, a high throughput of 30 wafer/h can be achieved.

Recently, the same research group integrated the lithography system with another plasmonic lens for the purpose of photolithography [100]. The plasmonic lens adopted is shown in Fig. 18. The metallic thin-film structure consisting of two concentric rings with an H-shaped aperture in their center is used as the plasmonic lens. With the 355 nm laser beam illumination, 50 nm lines width can be resolved on the TeO_x based thermal resist with a speed of about 10 m/s. It is said that the flying head in this work can carry up to 16,000 lenses within 2 nm gap tolerance. So the throughput can be greatly enhanced.

In addition, plasmonic interference lithography, which is an important part of plasmonic part, is another maskless lithography technique. Conventional plasmonic interference lithography scheme created on the basis of attenuated total reflection-coupling mode has three important components: a high refractive index prism, a metal layer, and the photoresist coated on substrate. A high refractive index is preferred because the higher refractive index of a prism leads to a smaller critical resonance angle. And it was demonstrated that the finer experimental results are easy to achieve at smaller incident angle [101]. Using this type of lithography system, 1D patterns using two-beam interference and 2D patterns using four-beam interference have been demonstrated [101–111]. The interferential beams are

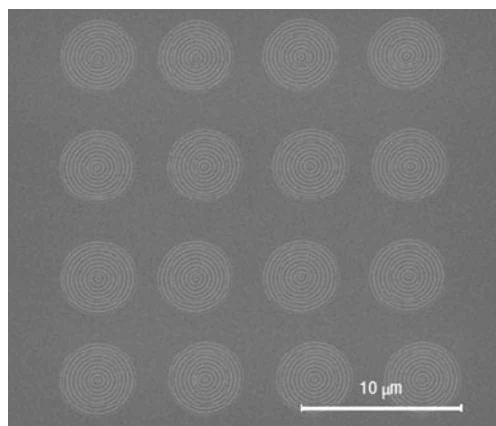

Fig. 17 SEM image of an array of plasmonic lens. Reprinted with permission from [99]

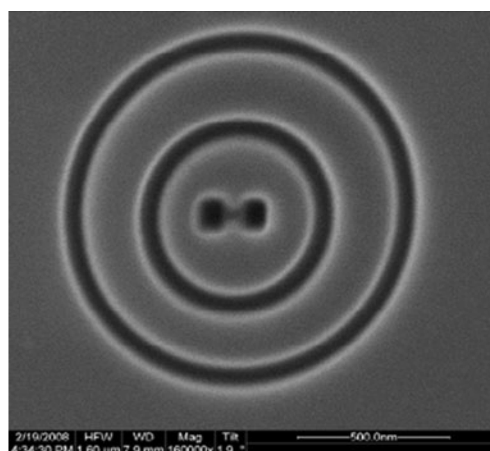

Fig. 18 SEM picture of the plasmonic lens adopted by Pan et al. Reprinted with permission from [100]

generally constituted from the first order diffraction light generated from the grating diffraction. In the conventional interference lithography, the photoresist and metal layer must be in contact closely. Therefore, the surface of the metal film and resist film are easily damaged or polluted. Furthermore, oxidation of the metal film is another problem due to exposure in air. To overcome these disadvantages, He et al. proposed and experimentally demonstrated a new approach based on backside-exposure technique [112]. The structure of this system composes a prism, matching fluid layer and glass substrate, Ag film and resist layer. This new structure not only prevents the damage and pollution but also eliminates the high refractive index prism from the system. Using this method, interference fringes with feature size below 65 nm were experimentally obtained. The throughput of interference lithography is quite high and the image quality is acceptable. But it is applicable only to periodic and quasiperiodic patterns, which limits its applications [111].

Finally, we supplemented a quantum effect-based new optical method which can realize the subwavelength lithography [113]. The method is similar to the traditional lithography but adding a critical step before dissociating the chemical bound of the photoresist. The subwavelength pattern is achieved by inducing the multi-Rabi oscillation between the two atomic levels. The proposed method does not require multiphoton absorption and the entanglement of photons. Initially, the molecules are in the ground state. Then two laser pulses with different frequencies were sequentially turned on. The first laser pulse, whose frequency is resonant with the energy difference between the two ground states, will induce Rabi oscillations between these two states. After that, the second laser pulse was turned on, and it will only dissociate the molecules that are in the excited states but not those in the ground states. The molecules that are dissociated will change their chemical properties, especially the solubility. The resulting patterns of the photoresist will thus depend on the spatial distribution of the excited state induced by the first laser pulse.

It is worthy to point out that as an alternative lithography technique, extreme-ultraviolet lithography at 13.5 nm is expected to be possibly introduced in high-volume semiconductor chip production over the next 3 years. Research is now underway to investigate sub-10 nm light sources that could support lithography over the coming decades [114]. An extension of this technology could be an alternative option for next-generation sub-13.5-nm lithography. Many of the technical issues, such as target regeneration and high-repetition rate operation, are already solved. However, improving the low conversion efficiency (about 0.5% for 2.48 nm) remains a critical point. Moreover, high expenditure is a drawback issue in comparison to plasmonic nanolithography technique.

Comparison Between Different Plasmonic Lithography Methods

The three nanolithography methods have been reviewed in details in above sections. Below gives a comparison of three different plasmonic lithography methods.

Generally speaking, the plasmonic contact lithography can get a higher resolution using masks with ridged shape apertures. Although large-area lithography can be realized through the step and repeat exposure and the production is relatively high, it still cannot satisfy the industrial requirement. In addition, the fabrication of conformable masks is complex and the cost is rather high. Intimate contact, which is assured by the external force sometimes, could cause the severe damage on the mask and substrate. The complexity in conjunction with the rigid exposure requirement of intimate contact between mask and substrate limits its further applications in many aspects. Researches on the new kind masks, such as elastic masks, can be done to consummate this method. Furthermore, the environment should be maintained rigidly clean in the process of lithography since any particles may affect the experiment result and even destroy the experiment.

In comparison to the contact lithography, the planar lens lithography relaxes the complexity of process control without the requirement of intimate contact between the mask and substrate. Thus, the masks and substrates can be prevented from being destroyed. But the superiority is restrained by the limited working distance (a few tens of nanometers or even less). Therefore, the research on the superlens with larger working distance should be made in future. In addition, this method is relatively underdeveloped compared with the contact lithography. It is commonly known that the resolution of this method is inferior to plasmonic contact lithography. Researches should be made to enhance the resolution.

Plasmonic direct writing nanolithography is considered as the most promising technique for its flexibility and low cost. In addition, it is a maskless lithography method. Therefore, it avoids all the complexity aroused by the masks. Arbitrary patterns with the resolution as small as 50 nm ($\lambda/8$, λ=405 nm) has been demonstrated by using this method. In addition, plasmonic direct writing lithography can be implemented in air and there is no such rigid environment requirement as the plasmonic contact lithography. Without the requirement of vacuum environment, the experiments are relatively easy to implement and it is a great superiority of this method. Forming arbitrary patterns and working in normal environment are the two superiorities of this method over former two lithography techniques. One of issues of the direct writing method is the low throughput. However, to expose the spinning substrate with flying plasmonic lens has the potential to achieve a

throughput that is two to five orders of magnitude higher than other maskless lithography and thus to be able to satisfy the industrial requirement. However, issues for flying plasmonic nanolithography like pattern data management, lithography linewidth control, pattern overlay, and resist defect reduction are still need to be addressed to apply this technology for nanomanufacturing industry.

Summary

In this article, we reviewed a technology of plasmonic nanolithography in three catalogs: contact nanolithography, planar lens nanolithography, and direct writing nanolithography. Some experiments about the three kinds of lithography techniques are presented and the comparison between them is also made. From the analysis presented above, we can conclude that the higher resolution is the unique superiority of plasmonic lithography. And further studies need to be done to address the issues of plasmonic nanolithography like lower throughput, pattern relay, and others to introduce the technology into the real nanomanufacturing industry. In summary, plasmonic nanolithography is one of the most promising techniques for next generation nanolithography and it has the potential to be applied in mass production.

Acknowledgments This work is supported by the National Natural Science Foundation of China with grant numbers of 90923036, 609770410, 60877021, and 61077010. The financial support from the 100 Talents Program of Chinese Academy of Sciences is acknowledged as well.

References

1. Vieu C, Carcenac F, Pépin A, Chen Y, Mejias M, Lebib A, Manin-Ferlazzo L, Couraud L, Launois H (2000) Electron beam lithography: resolution limits and applications. Appl Surf Sci 164:111–117
2. Chou SY, Krauss PR, Renstrom PJ (1995) Imprint of sub-25 nm vias and trenches in polymers. Appl Phys Lett 67(21):3114–3116
3. Kim K-H, Ke C, Moldovan N, Espinosa HD (2003) Proceedings of the 4th International Symposium on MEMS and Nanotechnology, the 2003 SEM Annual Conference and Exposition on Experimental and Applied Mechanics, June 2–4, Charlotte, North Carolina, Session 52. Paper 191:235–238
4. Wilson DL, Martin R, Hong S, Cronin-Golomb M, Mirkin CA, Kaplan DL (2001) Surface organization and nanopatterning of collagen by dip-pen nanolithography. PNAS 98:13660–13664
5. Cheng X, Guo LJ (2004) A combined-nanoimprint-and-photolithography patterning technique. Microelectron Eng 71:277–282
6. Yablonovitch E, Vrijen RB (1999) Optical projection lithography at half the Rayleigh resolution limit by two-photon exposure. Opt Eng 38(2):334–338
7. Crisalle OD, Keifling SR, Seborg DE, Mellichamp DA (1992) A comparison of the optical projection simulators in SAMPLE and PHOLITH. IEEE Trans Semicond Manuf 5:14–26
8. Chan SH, Wong AK, Lam EY (2008) Initialization for robust inverse synthesis of phase-shifting masks in optical projection lithography. Opt Express 16(19):14746–14760
9. Spille E, Feder R (1977) X-ray lithography. Top Appl Phys 22:35–92
10. Taylor JS, Sommargren GE, Sweeney DW, Hudyma RM (1998) Fabrication and testing of optics for EUV projection lithography. SPIE 3331:580–590
11. Menon R, Gil D, Smith HI (2006) Experimental characterization of focusing by high-numerical-aperture zone plates. J Opt Soc Am A 23(3):567–571
12. Smith HI (1996) A proposal for maskless, zone-plate-array nanolithography. J Vac Sci Technol B 14(6):4318–4322
13. Menon R, Patel A, Moon EE, Smith HI (2004) Alpha-prototype system for zone-plate-array lithography. J Vac Sci Technol B 22 (6):3032–3037
14. Smith HI, Menon R, Patel A, Chao D, Walsh M, Barbastathis G (2006) Zone-plate-array lithography: a low-cost complement or competitor to scanning-electron-beam lithography. Microelectron Eng 83:956–961
15. Menon R, Walsh M, Galus M, Chao D, Patel A, Smith HI (2005) Maskless lithography using diffractive-optical arrays, Frontiers in Optics, Tucson, Arizona Methodologies of Optical Design III (FWU).
16. Menon R, Patel A, Gil D, Smith HI (2005) Maskless lithography, Materials today ISSN:1369 7021, 26–33.
17. Yang L, Akhatov I, Mahinfalah M, Jang BZ (2007) Nano-fabrication: a review. J Chin Inst Eng 30(3):441–446
18. Kuwahara M, Nakano T, Tominaga J, Lee MB, Atoda N (2000) A new lithography technique using super-resolution near-field structure. Microelectron Eng 53:535–538
19. Goodberlet JG, Kavak H (2002) Patterning sub-50 nm features with near-field embedded-amplitude masks. Appl Phys Lett 81 (7):1315–1317
20. Ito T, Ogino M, Yamada T, Inao Y, Yamaguchi T, Mizutani N, Kuroda R (2005) Fabrication of sub-100 nm patterns using near-field mask lithography with ultra-thin resist process. J Photopolym Sci Technol 18(3):435–441
21. Ito T, Yamada T, Inao Y, Yamaguchi T, Mizutani N, Kuroda R (2006) Fabrication of half-pitch 32 nm resist patterns using near-field lithography with a-Si mask. Appl Phys Lett 89:033113(1)–03113(3)
22. Inao Y, Nakasato S, Kuroda R, Ohtsu M (2007) Near-field lithography as prototype nanofabrication tool. Microelectron Eng 84:705–710
23. Zhang YK, Dong XC, Du JL, Wei XZ, Shi LF, Deng QL, Du CL (2010) Nanolithography method by using localized surface plasmon mask generated with polydimethylsiloxane soft method on thin metal film. Opt Lett 35(13):2143–2145
24. Srituravanich W, Durant S, Lee H, Sun C, Zhang X (2005) Deep subwavelength nanolithography using localized surface plasmon modes on planar silver mask. J Vac Sci Technol B 23(6):2636–2639
25. Hicks EM, Zhang XY, Zou SL, Lyandres O, Spears KG, Schatz GC, Duyne RPV (2005) Plasmonic properties of film over nanowell surface fabricated by nanospheres lithography. J Phys Chem B 109:22351–22358
26. Degiron A, Ebbesen TW (2005) The role of localized surface plasmon modes in the enhanced transmission of periodic subwavelength apertures. J Opt A Pure Appl Opt 7:90–96
27. Alkaisi MM, Blaikie RJ, McNab SJ (2001) Nanolithography in the evanescent near field. Adv Mater 13(12–13):877–887
28. Srituravanich W, Fang N, Sun C, Luo Q, Zhang X (2004) Plasmonic nanolithography. Nano Lett 4(6):1085–1088
29. Srituravanich W, Fang N, Durant S, Ambati M, Sun C, Zhang X (2004) Sub-100 nm lithography using ultrashort wavelength of surface plasmons. J Vac Sci Technol B 22(6):3475–3478

30. Shao DB, Chen SC (2008) Surface plasmon assisted contact scheme nanoscale photolithography using an UV lamp. J Vac Sci Technol B 26(1):227–231
31. Zayats AV, Smolyaninov II (2006) High-optical-throughput individual nanoscale aperture in a multilayered metallic film. Opt Lett 31(3):398–400
32. Xiong Y, Liu ZW, Zhang X (2008) Projecting deep-subwavelength patterns from diffraction-limited masks using metal-dielectric multilayers. Appl Phys Lett 93:111116(1)–111116(3)
33. Xu X, Jin EX, Uppuluri SM, Wang L (2007) Concentrating light into nanometer domain using nanoscale ridge apertures and its application in laser-based nanomanufacturing. J Phys Conf Ser 59:273–278
34. Grober RD, Schoelkopf RJ, Prober DE (1997) Optical antenna: towards a unity efficiency near-field optical probe. Appl Phys Lett 70(11):1354–1356
35. Kinzel EC, Xu X (2009) High efficiency excitation of plasmonic waveguides with vertically integrated resonant bowtie apertures. Opt Express 17(10):8036–8045
36. Kim S, Jin J, Kim Y-J, Park I-Y, Kim Y, Kim S-W (2008) High-harmonic generation by resonant plasmon field enhancement. Nature 435:757–760
37. Jin EX, Xu X (2005) Obtaining super resolution light spot using surface plasmon assisted sharp ridge nanoaperture. Appl Phys Lett 86:111106(1)–111106(3)
38. Wang L, Uppuluri SM, Jin EX, Xu XF (2006) Nanolithography using high transmission nanoscale bowtie apertures. Nano Lett 6 (3):361–364
39. Ueno K, Takabatake S, Nishijima Y, Mizeikis V, Yokota Y, Misawa H (2010) Nanogap-assisted surface plasmon nano-lithography. J Phys Chem Lett 1:657–662
40. M-H Wu, Whitesides GM (2001) Fabrication of arrays of two-dimensional micropatterns using microsphere as lenses for projection photolithography. Appl Phys Lett 78(16):2273–2275
41. Sathiyamoorthy K, Sidharthan R, Sreekanth KV, Murukeshan VM (2010) Dye assisted enhanced transmission in near field optical lithography. Opt Commun 283:5245–5249
42. Kik PG, Martin AL, Maier SA, Atwater HA (2002) Metal nanoparticle arrays for near field optical lithography. Proc SPIE 4810:7–13
43. Pendry JB (2000) Negative refraction makes a perfect lens. Phys Rev Lett 85(18):3966–3969
44. Zhang X, Liu ZW (2008) Superlens to overcome the diffraction limit. Nat Mater 7:435–441
45. Chatterjee R, Panoiu NC, Liu K, Dios Z, Yu MB, Doan MT, Kaufman LJ, Osgood RM, Wong CW (2008) Achieving sub-diffraction imaging through bound surface states in negative-refracting photonics crystals at the near-infrared, American Physical Society March Meeting paper D35.00003.
46. Shvets G (2003) Photonic approach to making a material with a negative index of refraction. Phys Rev B 67:035109(1)–035109(8)
47. Shalaev VM (2007) Optical negative-index metamaterials. Nat Photonics 1:41–48
48. Jaksic Z, Vasiljevic-Radovic D, Maksimovic M, Sarajlic M, Vujanic A, Djuric Z (2006) Nanofabrication of negative refractive index metasurfaces. Microelectron Eng 83:1786–1791
49. Aydin K, Bulu I, Ozbay E (2007) Subwavelength resolution with a negative-index metamaterial superlens. Appl Phys Lett 90:254102(1)–254102(3)
50. Ma CB, Liu ZW (2010) Focusing light into deep subwavelength using metamaterial immersion lenses. Opt Express 18 (5):4838–4844
51. Tamma VA, Joshi S, Park W (2010) Optical frequency negative-index material based on silver nanocluster metamaterial, photonic metamaterials and plasmonics. Metamaterials III.
52. Korobkin D, Urzhumov Y, Shvets G (2006) Enhanced near-field resolution in midinfrared using metamaterials. J Opt Soc Am B 23(3):468–478
53. Fu YQ, Zhou XL (2010) Plasmonic lenses: a review. Plasmonics 5:287–310
54. Fang N, Liu ZW, Yen T-J, Zhang X (2003) Opt Express 11 (7):682–687
55. Yang XF, Liu Y, Ma JX, Cui JH, Xing H, Wang W, Wang CB, Luo XG (2008) Broadband super-resolution imaging by a superlens with unmatched dielectric medium. Opt Express 16 (24):19686–19694
56. Cai WS, Genov DA, Shalaev VM (2005) A superlens based on metal-dielectric composites. Phys Rev B 72:193101(1)–193101 (15)
57. Liu ZW, Fang N, Yen T-J, Zhang X (2003) Rapid growth of evanescent wave by a silver superlens. Appl Phys Lett 83 (25):5184–5186
58. Anantha Ramakrishna S, Pendry JB (2003) Removal of absorption and increase in resolution in a near-field lens via optical gain. Phys Rev B 67:201101(1)–201101(4)
59. Melville DOS, Blaikie RJ, Wolf CR (2004) Submicron imaging with a planar silver lens. Appl Phys Lett 84(22):4403–4405
60. Melville DOS, Blaikie RJ (2005) Super-resolution imaging through a planar silver layer. Opt Express 13(6):2127–2134
61. Blaikie RJ, Melville DOS, Alkaisi MM (2006) Super-resolution near-field lithography using planar silver lenses: a review of recent developments. Microelectron Eng 83:723–729
62. Moore CP, Arnold MD, Bones PJ, Blaikie RJ (2008) Image fidelity for single-layer and multi-layer silver superlenses. J Opt Soc Am A 25(4):911–918
63. Fang N, Lee H, Sun C, Zhang X (2005) Sub-diffraction-limited optical imaging with a silver superlens. Science 308:534–537
64. Lee H, Xiong Y, Fang N, Srituravanich W, Durant S, Ambati M, Sun C, Zhang X (2005) Realization of optical superlens imaging below the diffraction limit. New J Phys 7(255):1–16
65. Chaturvedi P, Wu W, Logeeswaran VJ, Yu ZN, Saif Islam M, Wang SY, Williams RS, Fang NX (2010) A smooth optical superlens. Appl Phys Lett 96:043102(1)–043102(3)
66. Shi Z, Kochergin V, Wang F (2009) 193 nm Superlens imaging structure for 20 nm lithography node. Opt Express 17 (14):11309–11314
67. Shi Z, Kochergin V, Wang F (2009) Depth-of-focus(DoF) analysis of a 193 nm superlens imaging structure. Opt Express 17(22):20538–20545
68. Xu T, Fang L, Ma J, Zeng B, Liu Y, Cui J, Wang C, Feng Q, Luo X (2009) Localizing surface plasmons with a metal-cladding superlens for projecting deep-subwavelength patterns. Appl Phys B 97:175–179
69. Liu ZW, Durant S, Lee H, Pikus Y, Xiong Y, Sun C, Zhang X (2007) Experimental studies of far-field superlens for sub-diffraction optical imaging. Opt Express 15(11):6947–6954
70. Liu ZW, Durant S, Lee H, Pikus Y, Fang N, Xiong Y, Sun C, Zhang X (2007) Far-field optical superlens. Nano Lett 7(2):403–408
71. Milster T, Chen T, Nam D, Schlesinger E (2004) Maskless lithography with solid immersion lens nano probes. Proc SPIE 5567:545–556
72. Bae JH, Ono T, Esashi M (2003) Scanning probe with an integrated diamond heater element for nanolithography. Appl Phys Lett 82(5):814–816
73. Eckert R, Freyland JM, Gersen H, Heinzelmann H, Schürmann G, Noell W, Staufer U, de Rooij NF (2000) Near-field fluorescence imaging with 32 nm resolution based on microfabricated cantilevered probes. Appl Phys Lett 77(23):3695–3697
74. Hamada M, Eguchi T, Akiyama K, Hasegawa Y (2008) Nanoscale lithography with frequency-modulation atomic force microscopy. Rev Sci Instrum 79:123706(1)–123706(4)

75. Tian F, Yang GG, Bai J, Zhou QF, Hou CL, Xu JF, Liang YY (2010) Subwavelength-resolution direct writing using submicron-diameter fibers. Chin Opt Lett 8(3):326–328
76. Tian F, Yang GG, Bai J, Xu JF, Hou CL, Liang YY, Wang KW (2009) Laser direct writing using submicron-diameter fibers. Opt Express 17(22):19960–19968
77. Ryu KS, Wang XF, Shaikh K, Bullen D, Goluch E, Zou J, Liu C, Mirkin CA (2004) Integrated microfluidic linking chip for scanning probe nanolithography. Appl Phys Lett 85(1):136–138
78. Kim K-H, Moldovan N, Ke C, Espinosa HD, Xiao XC, Carlisle JA, Auciello O (2005) Novel ultrananocrystalline diamond probes for high-resolution low-wear nanolithographic techniques. Small 1(8–9):866–874
79. Stockman MI (2004) Nanofocusing of optical energy in tapered plasmonic waveguides. Phys Rev Lett 93(13):137404 (1)–137404(4)
80. Ghislain LP, Elings VB, Crozier KB, Manalis SR, Minne SC, Wilder K, Kino GS, Quate CF (1999) Near-field photolithography with a solid immersion lens. Appl Phys Lett 74(4):501–503
81. Zhang YJ, Suyama T, Shi TZ (2010) Near-field double-spot photolithography with subwavelength spacing. Opt Commun 283:3022–3025
82. Kwon S, Kim P, Jeong S, Chang W, Chun C, Kim D-Y (2005) Fabrication of nano dot and line arrays using NSOM lithography. J Opt Soc Korea 9(1):16–21
83. Minh PN, Ono T, Esashi M (2000) High throughput aperture near-field scanning optical microscopy. Rev Sci Instrum 71 (8):3111–3116
84. Leggett GJ (2006) Scanning near-field photolithography-surface photochemistry with nanoscale spatial resolution. Chem Soc Rev 35:1150–1161
85. Tarun A, Daza MRH, Hayazawa N, Inouye Y, Kawata S (2002) apertureless optical near-field fabrication using an atomic force microscope on photoresist. Appl Phys Lett 80(18):3400–3402
86. Raschke MB, Molina L, Elsaesser T, Kim DH, Knoll W, Hinrichs K (2005) Apertureless near-field vibrational imaging of block-copolymer nanostructures with ultrahigh spatial resolution. Chemphyschem 6:2197–2203
87. Dryakhlushin VF, Klimov AY, Rogov VV, Vostokov NV (2005) Near-field optical lithography method for fabrication of the nanodimensional objects. Appl Surf Sci 248:200–203
88. Shao DB, Li SF, Chen SC (2004) Near-field-enhanced, mold-assisted, parallel direct nanostructuring of a gold thin film on glass. Appl Phys Lett 85(22):5346–5348
89. Hwang DJ, Cheimmalgi A, Grigoropoulos CP (2006) Ablation of thin metal films by short-pulsed lasers coupled through near-field scanning optical microscopy probes. J Appl Phys 99:044905(1)–044905(11)
90. Haefliger D, Stemmer A (2004) Writing subwavelength-sized structures into aluminium films by thermo-chemical aperture-less near-field optical microscopy. Ultramicroscopy 100:457–464
91. Kim Y, Park S, Lee E, Hahn JW (2008) Nanopatterning with a single high-transmission nano-metal aperture system, Proc. of SPIE 69212 C(1)-C(8).
92. Wang Y, Srituravanich W, Sun C, Zhang X (2008) Plasmonic nearfield scanning probe with high transmission. Nana Lett 8 (9):3041–3045
93. Zhou LC, Gan QQ, Bartoli FJ, Dierolf V (2009) Direct near-field optical imaging of UV bowtie nanoantennas. Opt Express 17 (22):20301–20306
94. Jin EX, Xu XF (2006) Enhanced optical near field from a bowtie aperture. Appl Phys Lett 88:153110(1)–153110(3)
95. DuBay NM, Wang L, Kinzel EC, Uppuluri SMV, Xu X (2008) Nanopatterning using NSOM probes integrated with high transmission nanoscale bowtie aperture. Opt Express 16 (4):2584–2589
96. Latini G, Downes A, Fenwick O, Ambrosio A, Allegrini M, Daniel C, Silva C, Gucciardi PG, Patanè S, Daik R, Feast WJ, Cacialli F (2005) Optical probing of sample heating in scanning near-field experiments with apertured probes. Appl Phys Lett 86:011102(1)–011102(3)
97. Ambrosio A, Fenwick O, Cacialli F, Micheletto R, Kawakami Y, Gucciardi PG, Kang DJ, Allegrini M (2006) Shape dependent thermal effects in apertured fiber probes for scanning near-field optical microscopy. J Appl Phys 99:084303(1)–084303(6)
98. Kim Y, Kim S, Jung H, Lee E, Hahn JW (2009) Plasmonic nano lithography with a high scan speed contact probe. Opt Express 17(22):19476–19485
99. Srituravanich W, Pan L, Wang Y, Sun C, Bogy DB, Zhang X (2008) Flying plasmonic lens in the near field for high-speed nanolithography. Nat Nanotechnol 3:733–737
100. Pan L, Park Y-S, Xiong Y, Avila EU, Zeng L, Sun C, Bogy DB, Zhang X (2010) Flying plasmonic lens at near field for high speed nano-lithography. Proc. of SPIE 7637, 763713(1)–763713(6).
101. Niu XY, Qi YM, Wang JQ, Zhang ZY, Du JL, Guo YK, Shi RY, Gong M (2010) Approach of enhancing exposure depth for evanescent wave interference lithography. Microelectron Eng 87:1168–1171
102. Xiong W, Du JL, Fang L, Luo XG, Deng QL, Du CL (2008) 193 nm Interference nanolithography based on SPP. Microelectron Eng 85:754–757
103. Shi S, Zhang ZY, He MY, Li XP, Yang J, Du JL (2010) Analysis of surface-plasmon-polaritons-assisted interference imaging by using silver film with rough surface. Opt Express 18(10):10685–10693
104. Lim Y, Kim S, Kim H, Jung J, Lee B (2008) Interference of surface plasmon waves amd plasmon coupled waveguide modes for the patterning of thin film. IEEE J Quantum Electron 44 (4):305–311
105. Sreekanth KV, Murukeshan VM (2010) Large-area maskless surface plasmon interference for one- and two-dimensional periodic nanoscale feature patterning. J Opt Soc Am A 27 (1):95–99
106. Guo XW, Du JL, Guo YK (2006) Large-area surface-plasmon polaritons interference lithography. Opt Express 31(17):2613–2615
107. Murukeshan VM, Chua JK, Tan SK, Lin QY (2008) Modeling of subwavelength resist grating features fabricated by evanescent waves interference. Opt Eng 47(12):129001(1)–129001(9)
108. Doskolovich LL, Kadomina EA, Kadomin II (2007) Nanoscale photolithography by means of surface plasmon interference. J Opt A Pure Appl Opt 9:854–857
109. Sreekanth KV, Murukeshan VM (2010) Single-exposure maskless plasmonic lithography for patterning of periodic nanoscale grating features. J Micro/Nanolith MEMS MOEMS 9(2):023007 (1)–023007(4)
110. Fang L, Du JL, Guo XW, Wang JQ, Zhang ZY, Luo XG, Du CL (2008) The theoretic analysis of maskless surface plasmon resonant interference lithography by prism coupling. Chin Phys B 17(7):2499–2503
111. Chua JK, Murukeshan VM, Tan SK, Lin QY (2007) Four beams evanescent waves interference lithography for patterning of two dimensional features. Opt Express 15(6):3437–3451
112. He MY, Zhang ZY, Shi S, Du JL, Li XP, Li SH, Ma WY (2010) A practical nanofabrication method: surface plasmon polaritons interference lithography based on backside-exposure technique. Opt Express 18(15):15975–15980
113. Zeyang Liao, Al-Amri M, Suhail Zubairy M (2010) Quantum lithography beyond the diffraction limit via Rabi oscillations. Phys Rew Lett 105:183601
114. Tallents G, Wagenaars E, Pert G (2010) Optical lithography: lithography at EUV wavelengths. Nat Photonics 4:809–811